Electronic Supplementary Material (ESI) for Journal of Materials Chemistry C.

Supporting Information

Photoluminescent Manipulation of Phenoxazine Based Molecules via Regulating Conformational Isomerization, and Corresponding Electroluminescent Properties

Zong Cheng, Jixiong Liang, Zhiqiang Li, Tong Yang, Chunhui Lin, Xiaoyue Mu and Yue Wang**

Table of Contents

1. General Information

^{1}H NMR spectra were measured on a Bruker AVANCE III 500 MHz spectrometer with tetramethylsilane as the internal standard. Mass spectra were recorded on a Thermo Fisher ITQ1100 GC/MS mass spectrometer. Elemental analyses were performed on a flash EA 1112 spectrometer. The UV-Vis absorption spectra were recorded by a Shimadzu UV-2550 spectrophotometer. The emission spectra were recorded by a Shimadzu RF-5301 PC spectrometer. Both fluorescence and phosphorescent spectra at low temperature (77 K) were recorded by Ocean Optics QE Pro with a 375 nm Ocean Optics LLS excitation source. The absolute fluorescence quantum yields of solutions and films were measured on an Edinburgh FLS920 steady state fluorimeter utilizing an integrating sphere (excited at 340 nm). Fluorescence microscopy images were obtained on an Olympus BX51 fluorescence microscope. Differential scanning calorimetric (DSC) measurements were performed on a NETZSCH DSC204 instrument at a heating rate of 10 K min^{-1} under a nitrogen atmosphere. Thermogravimetric analyses (TGA) were performed on a TA Q500 thermogravimeter by measuring their weight loss while heating at a rate of 10 K min^{-1} from 25 to 900 °C under nitrogen. Electrochemical measurements were performed with a BAS 100W Bioanalytical electrochemical work station, using a platinum disk as working electrode, platinum wire as auxiliary electrode, and a porous glass wick Ag/Ag$^+$ as pseudo reference electrode with ferrocene/ferrocenium as the internal standard. The oxidation and reduction potentials were measured in CH_2Cl_2 and THF solution containing 0.1 M of n-Bu_4NPF_6 as a supporting electrolyte at a scan rate of 50 mV s^{-1}. Transient PL decay was investigated under vacuum using a FLS920 fluorescence lifetime measurement system with 365 nm LED excitation source. SEM (scanning electron microscopy) analysis was conducted on a JEOL JSM-6700F field-emission scanning electron microscope. Before imaging, all samples were coated with gold to prevent charging.

Theoretical Calculations method: The ground state geometries of gas state were fully optimized by B3LYP method including Grimme's dispersion correction with 6-31G(d,p) basis set using Gaussian 09 software package.[1-5] To verify that the optimized structure was the local minima on the S_0 energy surface, the vibrational frequencies at the optimized structures were also calculated using the same DFT method. HOMO and LUMO were visualized with Gaussview 5.0. The excited state properties were calculated by TD-DFT with the same theory level as DFT.

Single-Crystal Growth and X-ray Diffraction Analyses: The **PXZ-DCzBN** sheet crystal was prepared by slowly volatilizing a mixed solution of toluene, methanol, dichloromethane and water. The block-like **PXZ-DtCzBN** crystal was directly prepared by temperature-gradient vacuum sublimation. Diffraction data were collected on a Rigaku RAXIS-PRID diffractometer using the ω-scan mode with graphite monochromator Mo•K_α radiation. The structure was solved using SHELXT and refined with SHELXL.[6-7] Non-hydrogen atoms were refined anisotropically. The positions of hydrogen atoms were calculated and refined isotropically. CCDC 1912715-1912716 contains the supplementary crystallographic data for this paper, and the data can be obtained free of charge from The Cambridge Crystallographic Data Centre via "www.ccdc.cam.ac.uk/data_request/cif".

Device Fabrication and Characterization. Glass substrates pre-coated with indium tin oxide (ITO) with a sheet resistance of 15 Ω per square were thoroughly cleaned in an ultrasonic bath of tetrahydrofuran, detergent, deionized water, acetone and isopropyl alcohol and treated with plasma for 5 min in sequence. Organic layers were deposited onto the ITO-coated glass substrates by thermal evaporation under high vacuum ($<9 \times 10^{-5}$ Pa). Cathode was patterned using a shadow mask with an array of 2.0 mm × 2.5 mm openings. Deposition rates are 1 Å s^{-1} for organic materials, 0.1 Å s^{-1} for LiF, and 5 Å s^{-1} for Al, respectively. Electroluminescence (EL) spectra and luminance intensities were recorded by Photo Research PR655. The current density (J) and driving voltage (V) characteristics were measured by

Keithley 2400 simultaneously. External quantum efficiency (EQE) was calculated from the current density, luminance, and EL spectrum, assuming a Lambertian distribution.

Calculation Formulas for the Photophysical Parameters:

The calculation formulas for the rate constants of fluorescent (k_F), internal conversion (k_{IC}), inter-system crossing (k_{ISC}), TADF (k_{TADF}) and reverse intersystem crossing (k_{RISC}) are expressed as following listed:[8]

$$k_F = \Phi_F/\tau_F = \Phi_F k_P \quad (S1)$$

$$k_D = 1/\tau_{TADF} \quad (S2)$$

$$\Phi_{RISC} = \Phi_{TADF}/(1- \Phi_F) \quad (S3)$$

$$\Phi_F = k_F/(k_F + k_{ISC}) \quad (S4)$$

$$\Phi_{ISC} = k_{ISC}/(k_F + k_{ISC}) \quad (S5)$$

$$k_{TADF} = \Phi_{TADF}/(\Phi_{ISC}\, \tau_{TADF}) \quad (S6)$$

$$k_{RISC} = k_P\, k_D\, \Phi_{TADF}/(k_{ISC}\, \Phi_F) \quad (S7)$$

$$\Phi_{TADF}/\Phi_F = (\Phi_{ISC}\, \Phi_{RISC})/(1-\Phi_{ISC}\, \Phi_{RISC}) \quad (S8)$$

2. Synthesis

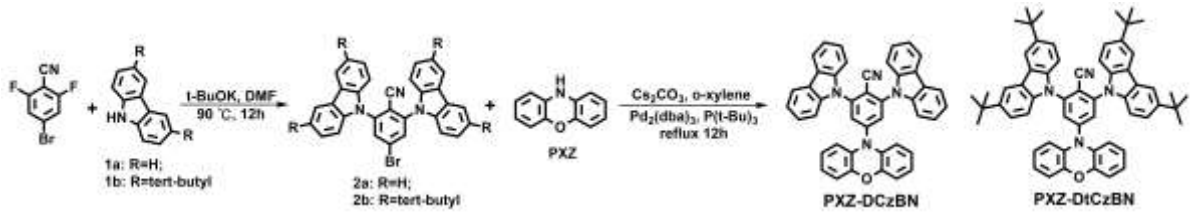

Scheme S1. Synthetic routes of **PXZ-DCzBN** and **PXZ-DtCzBN**.

The chemical reagents were purchased from *Energy Chemical Co*. and/or *J&K scientific Ltd. Co*., and used immediately without further purification. All reactions were carried out using Schlenk techniques under a nitrogen atmosphere. The syntheses process is as showed below in detail.

Synthesis of 4-bromo-2, 6-di(carbazol-9-yl)benzonitrile ***(compound 2a)****:* A mixture of t-BuOK (1.12g, 10 mmol) in 20 ml anhydrous N,N- dimethylformamide (DMF) was added into 20 ml DMF solution containing 9H-carbazole (1.25 g, 7.5 mmol) during 15 min. Then the system was stirred for 1 h at room temperature to fully activate the carbazole, after that, 4-bromo-2,6-difluorobenzonitrile (0.73 g, 3.33 mmol) in 8 ml anhydrous DMF solution was injected into the system during a 15 min timeframe. The system was cooled down to room temperature after reacting at 90°C for 12h. Then it was poured into ice water (1000 g) and filtered out to collect the white powder solid, which was dried in vacuum first then purified by column chromatography with using a mixture eluent of CH_2Cl_2/PE (1:2), resulting in a white solid (1.25 g). Yield: 73%. H NMR (500 MHz, Chloroform-d_1) δ/ppm: 8.15 (d, J = 7.3 Hz, 4H), 7.93 (s, 2H), 7.54 – 7.50 (m, 4H), 7.41 – 7.36 (m, 8H). ESI-MS (M): m/z: 511.22 $[M]^+$ (calcd: 511.07).

Synthesis of 4-bromo-2, 6-di(3,6-tert-butyl-carbazol-9-yl)benzonitrile ***(compound 2b)****:* A procedure similar to the synthesis of compound 2a was carried out except replacing carbazole with tert-butyl carbazole (2.10 g, 7.5 mmol), resulting in a white solid (2.24 g). Yield: 91%.

^{1}H NMR (500 MHz, DMSO-d_6) δ/ppm: 8.34 (s, 4H), 8.28 (s, 2H), 7.57 (d, *J* = 8.6 Hz, 4H), 7.41 (d, *J* = 8.7 Hz, 4H), 1.44 (s, 36H). ESI-MS (M): m/z: 735.27 $[M]^+$ (calcd: 735.32).

Synthesis of 2,6-di(9H-carbazol-9-yl)-4-(10H-phenoxazin-10-yl)benzonitrile ***(PXZ-DCzBN)****:* Anhydrous o-xylene (45 mL) was added into a flask containing compound 2a (1.21 g, 2.36 mmol), PXZ (0.606 g, 3.54 mmol), Cs_2CO_3 (3.07 g, 9.44 mmol), where $Pd_2(dba)_3$ (0.184 g, 0.2 mmol) was added after compound 2a and PXZ fully dissolved. Whereafter, tri-tert-butylphosphine (TTBP) (0.40 g, 0.2 mmol) was injected into the system, then it was stirred at the reflux temperature for 12 h. After cooling down to the ambient temperature, the resulting system was extracted with CH_2Cl_2 for 3 times. Then the organic layer was concentrated and purified by column chromatography with a mixture eluent of CH_2Cl_2/PE (1:1), resulting in a yellow solid (1.30 g) in 90% yield. ^{1}H NMR (500 MHz, DMSO-d_6) δ/ppm: δ 8.29 (d, J = 7.7 Hz, 4H), 8.19 (s, 2H), 7.68 (d, J = 8.2 Hz, 4H), 7.58 – 7.53 (m, 4H), 7.38 (t, J = 7.5 Hz, 4H), 6.88 (ddd, J = 8.2, 5.6, 3.4 Hz, 2H), 6.84 – 6.79 (m, 4H), 6.75 – 6.71 (m, 2H). ESI−MS m/z: 614.13 $[M]^+$ (calcd: 614.21) Anal. Calcd for $C_{43}H_{26}N_4O$: C, 84.02; H, 4.26; N, 9.11. Found: C, 84.12; H, 4.29; N, 9.01.

Synthesis of 2,6-bis(3,6-di-tert-butyl-9H-carbazol-9-yl)-4-(10H-phenoxazin-10-yl)benzonitrile ***(PXZ-DtCzBN)****:* A method similar to the synthesis of **PXZ-DCzBN** was implemented except that compound 2b (1.74 g, 2.36 mmol) was used instead of compound 2a, resulting in a yellow solid (1.98 g) in 85% yield. ^{1}H NMR (500 MHz, DMSO-d_6) δ/ppm: δ 8.34 (d, J = 2.0 Hz, 4H), 8.07 (s, 2H), 7.58 (dd, J = 8.7, 1.9 Hz, 4H), 7.52 (d, J = 8.6 Hz, 4H), 6.86 (ddd, J = 7.9, 5.6, 3.5 Hz, 2H), 6.82 – 6.75 (m, 4H), 6.63 – 6.57 (m, 2H), 1.43 (s, 36H).ESI−MS m/z: 838.46 $[M]^+$ (calcd: 838.46). Anal. Calcd for $C_{59}H_{58}N_4O$: C, 84.45; H, 6.97; N, 6.68. Found: C, 84.65; H, 6.77; N, 6.65.

3. Figures

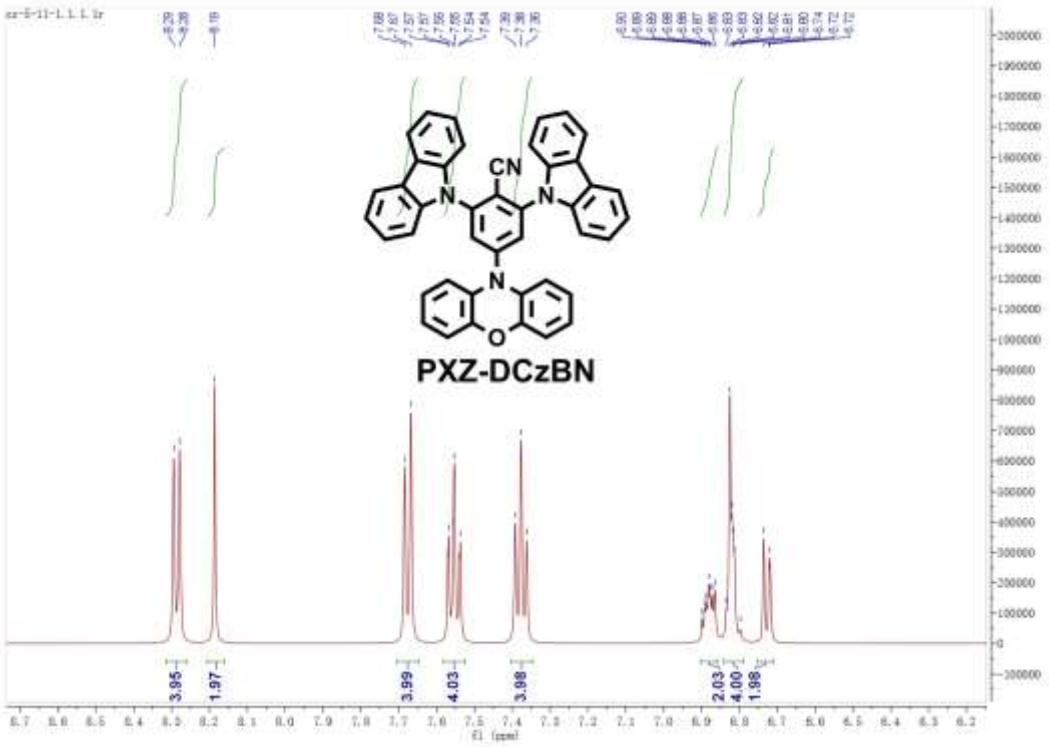

Fig. S1. ^{1}H NMR spectrum of **PXZ-DCzBN** in DMSO.

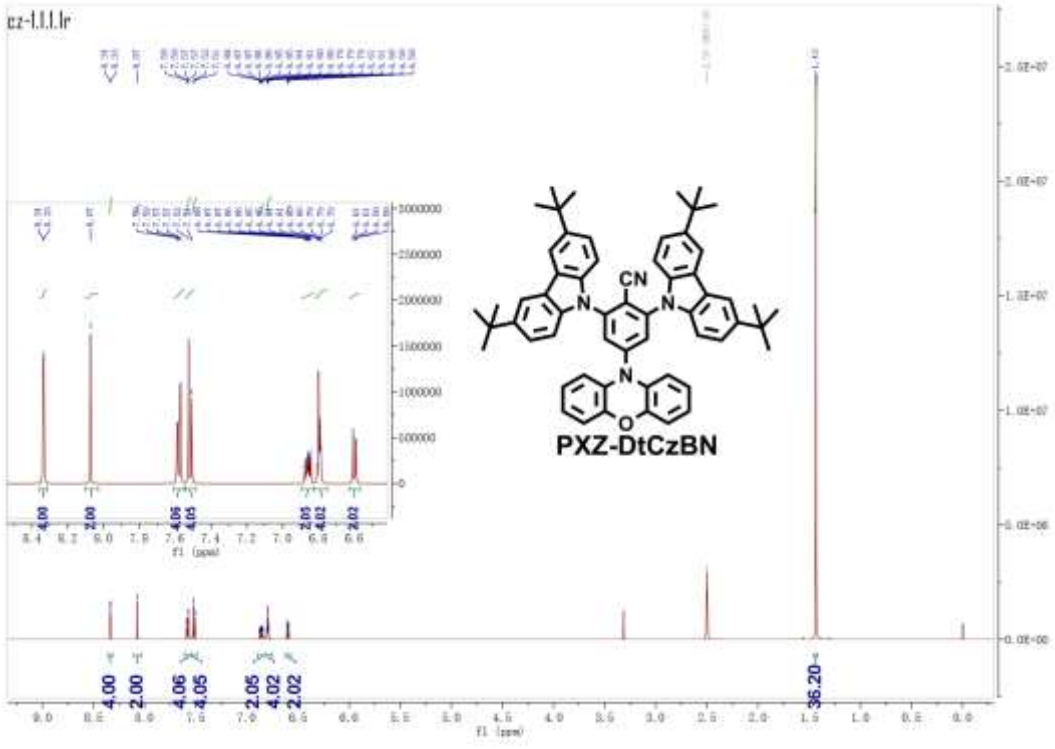

Fig. S2. ^{1}H NMR spectrum of **PXZ-DtCzBN** in DMSO.

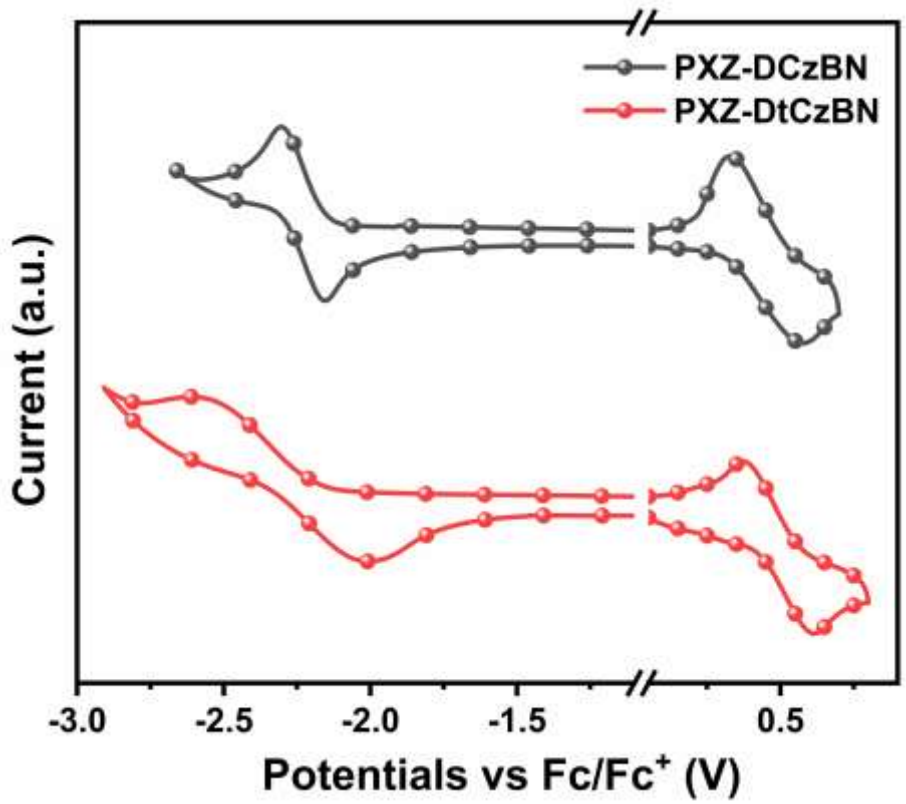

Fig. S3. Cyclic Voltammogram of **PXZ-DCzBN** and **PXZ-DtCzBN**.

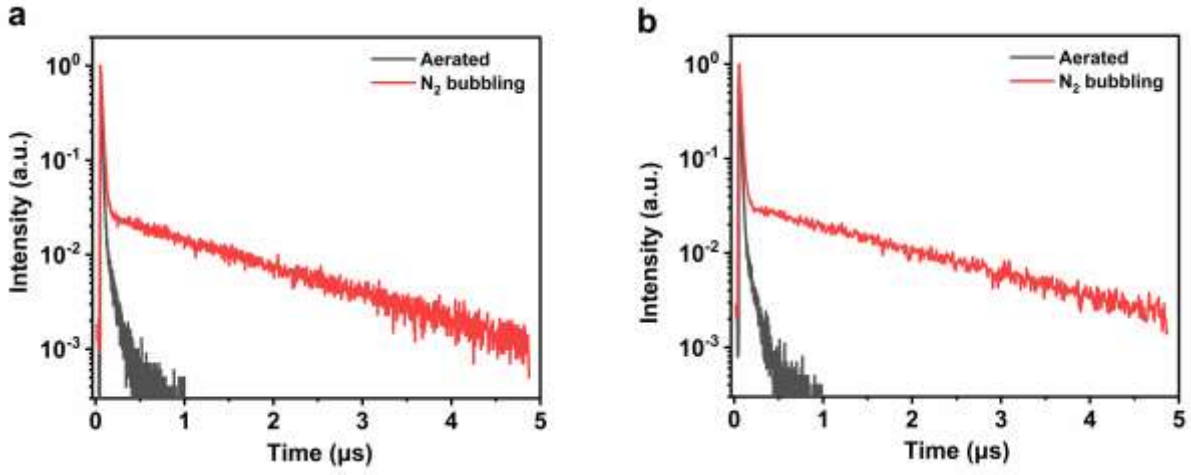

Fig. S4. Transient decay spectra of the toluene solution of a) **PXZ-DCzBN** and b) **PXZ-DtCzBN** at room temperature under ambient and N_2 bubbling condition.

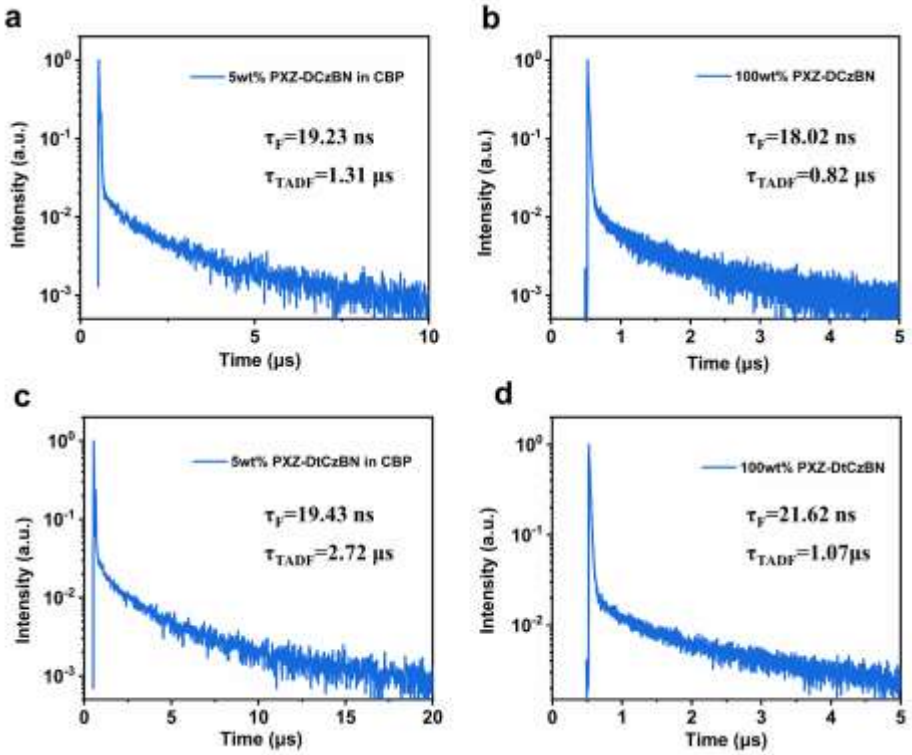

Fig. S5. Transient decay spectra of the **PXZ-DCzBN** in a) 5 wt% CBP doped film and b) non-doped film, and **PXZ-DtCzBN** c) 5 wt% CBP doped film and d) non-doped film.

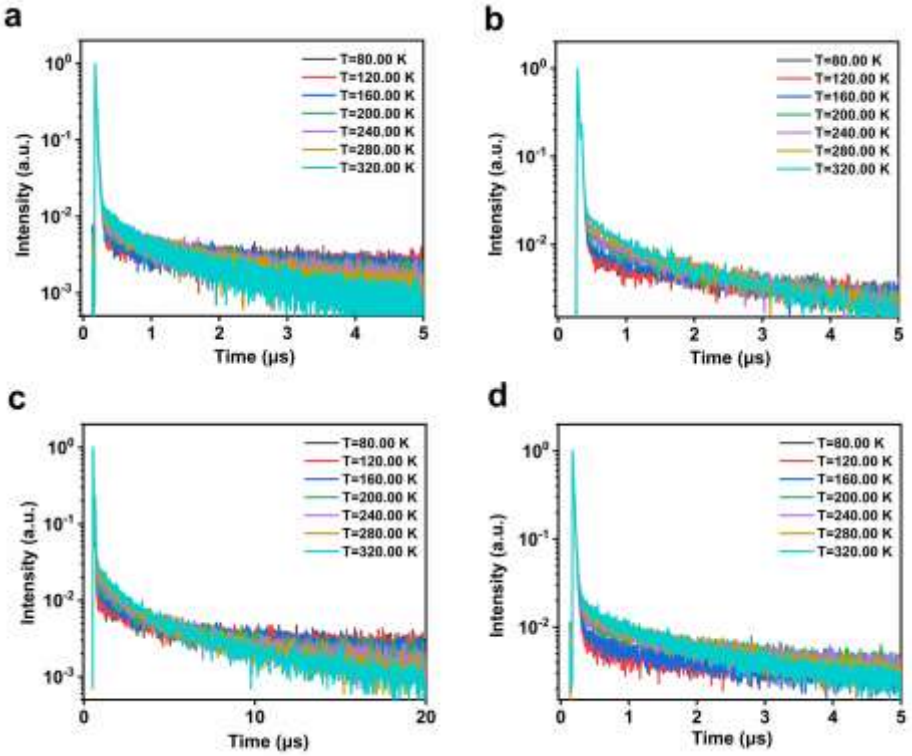

Fig. S6. Transient PL decay curves of a) 5 wt% **PXZ-DCzBN**: CBP film, b) **PXZ-DCzBN** neat film, c) 5 wt% **PXZ-DtCzBN**: CBP film, d) **PXZ-DtCzBN** neat film measured at 80-320K.

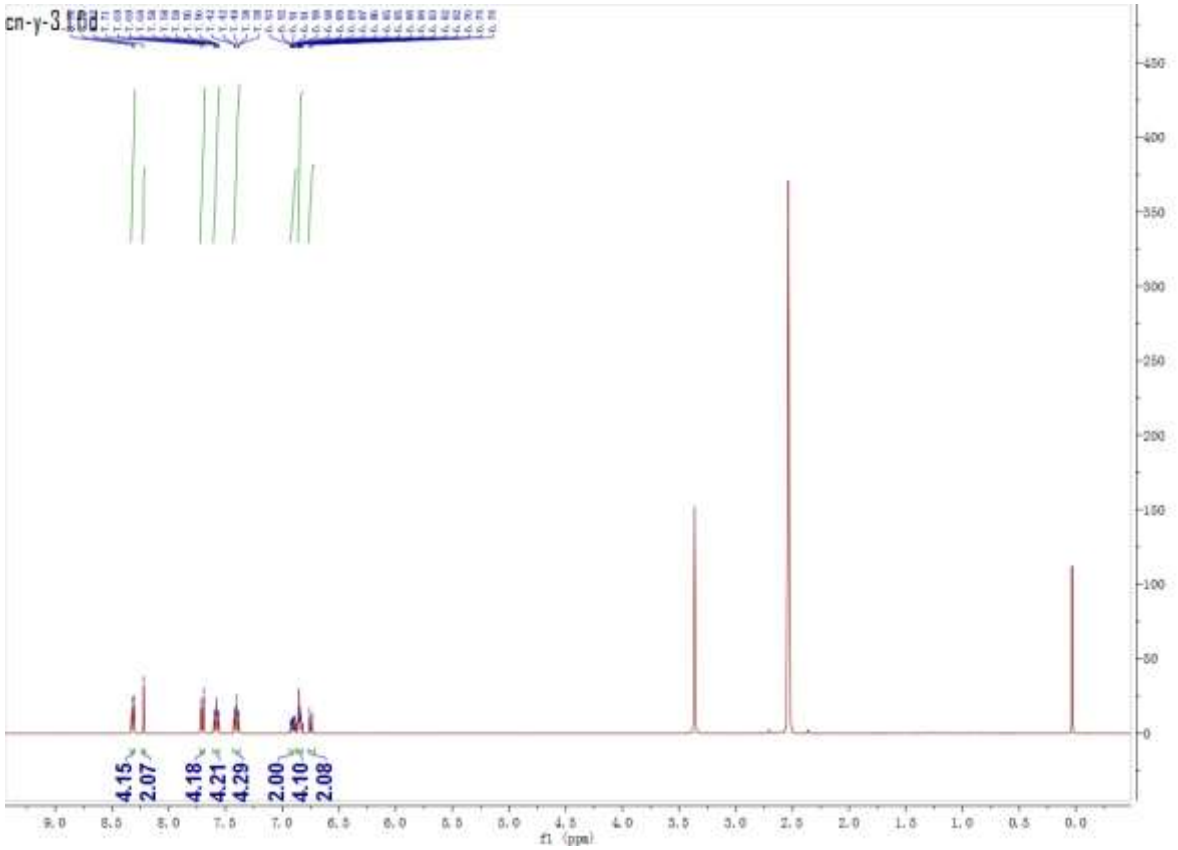

Fig. S7. ^{1}H NMR spectrum of YP in DMSO.

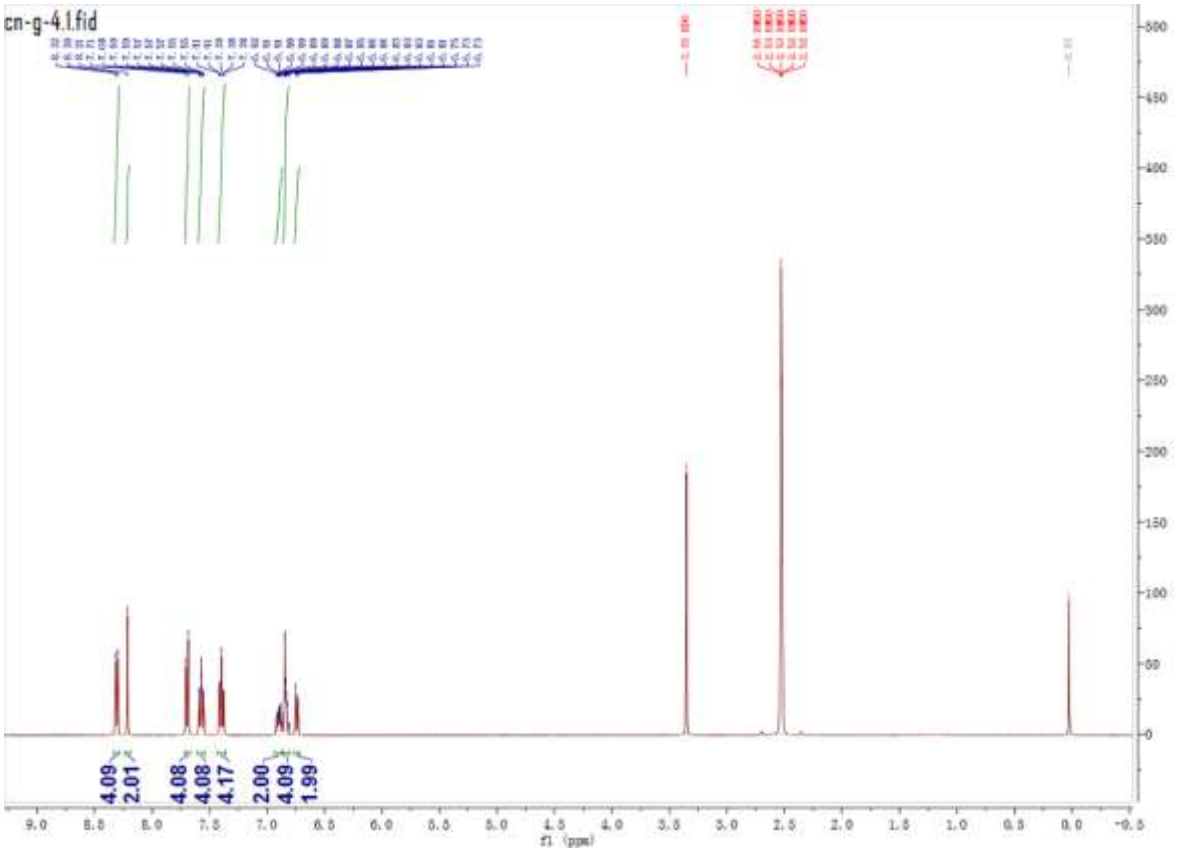

Fig. S8. ^{1}H NMR spectrum of GP in DMSO.

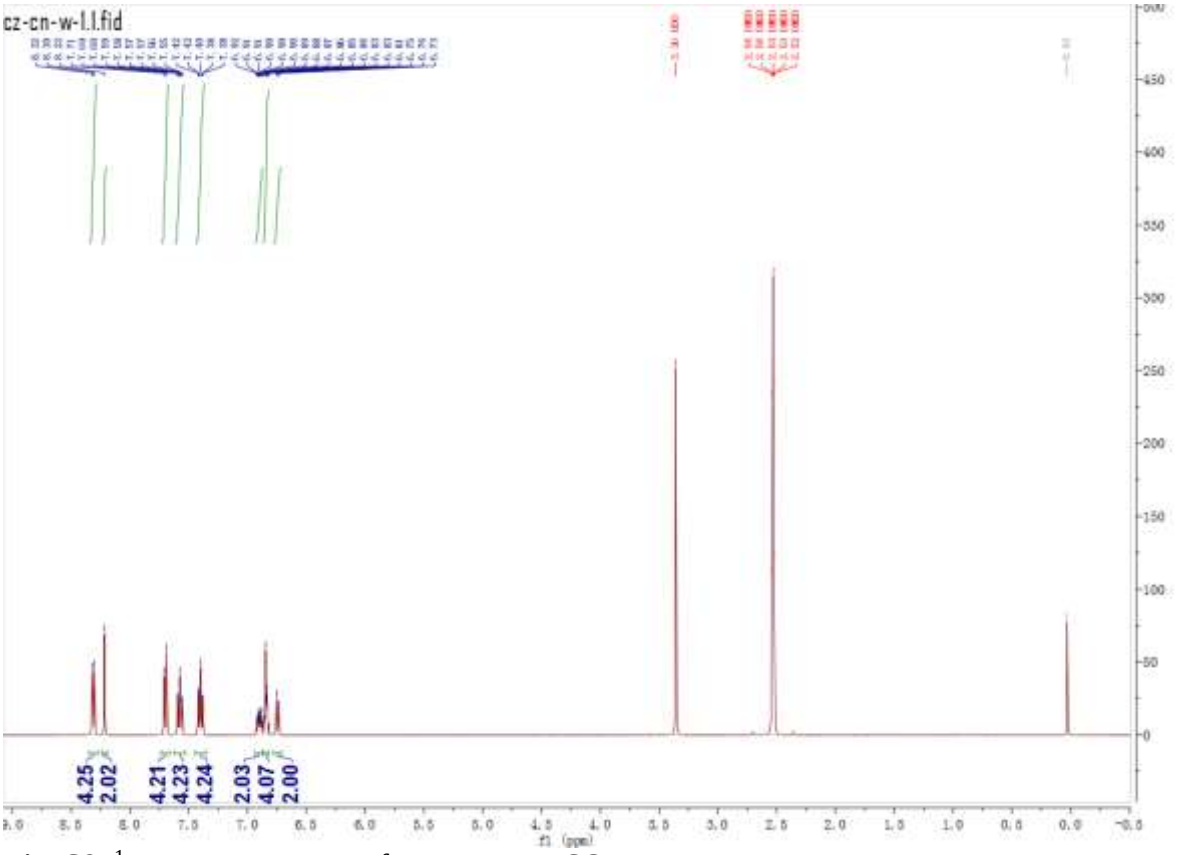

Fig. S9. ^{1}H NMR spectrum of WP-1 in DMSO.

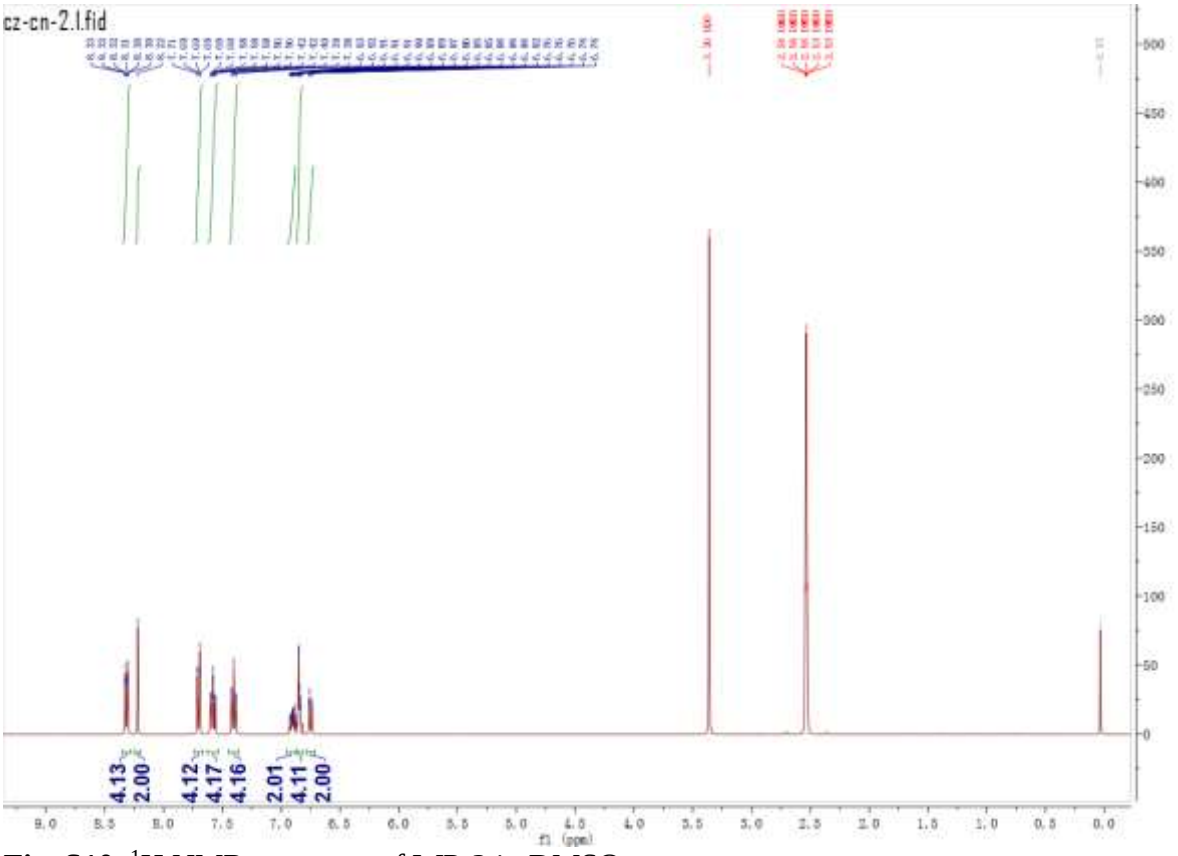

Fig. S10. ^{1}H NMR spectrum of WP-2 in DMSO.

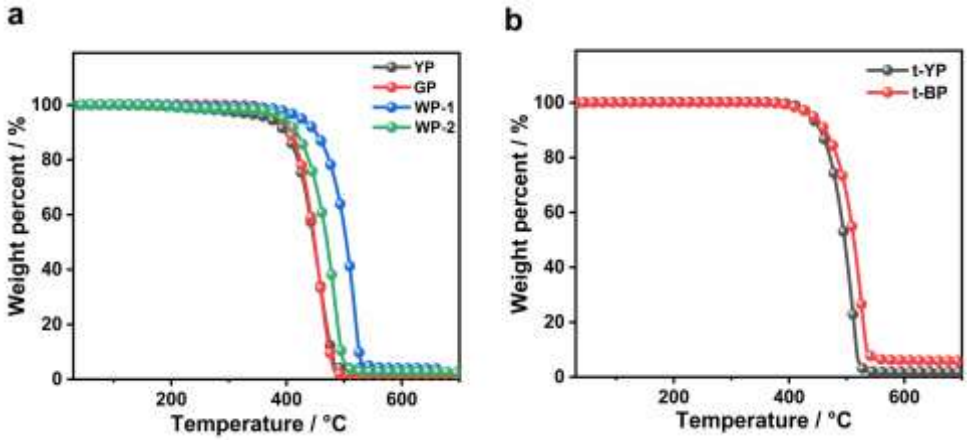

Fig. S11. TGA curves of different samples of a) **PXZ-DCzBN** and b) **PXZ-DtCzBN**.

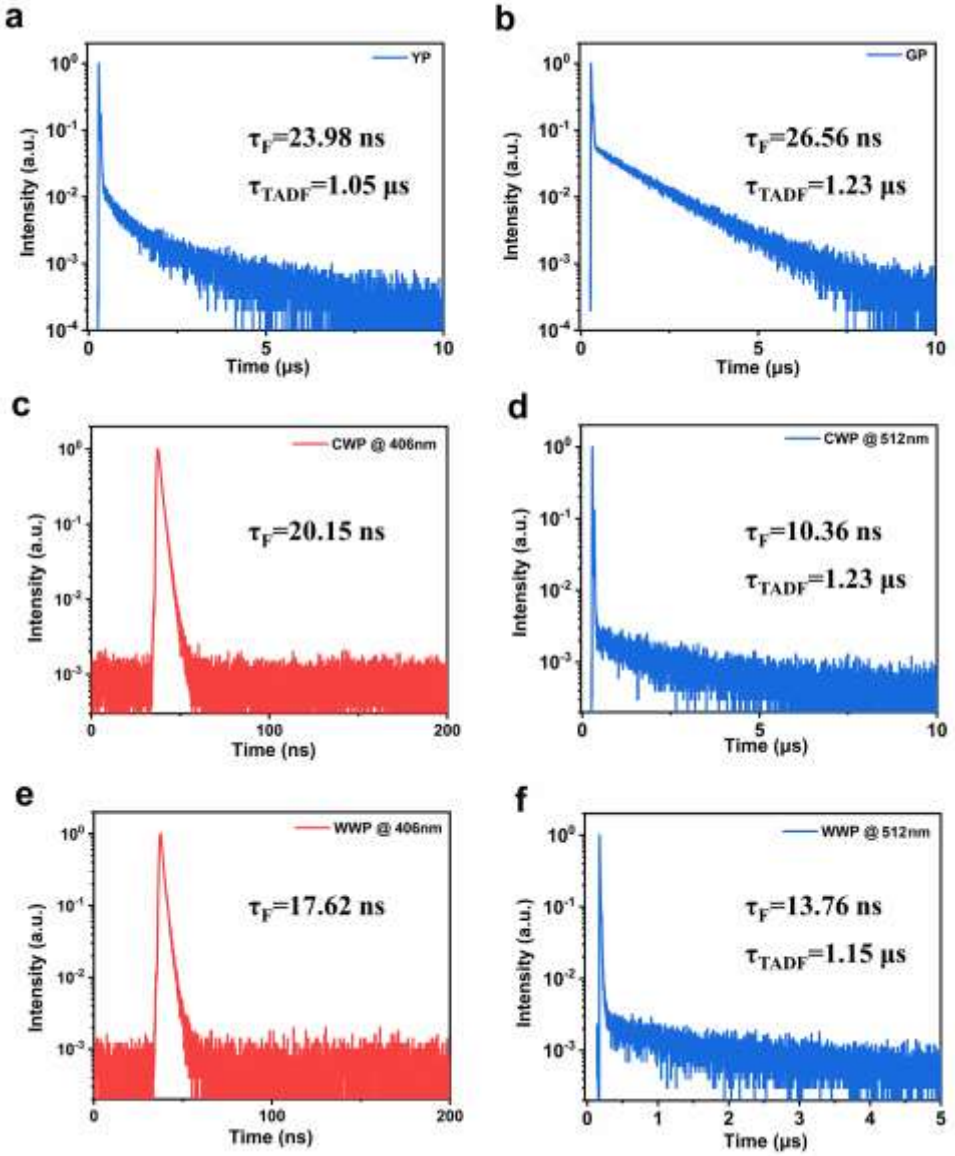

Fig. S12. Transient decay spectra of different samples of **PXZ-DCzBN**: a) YP, b) GP, c) WP-1 at 406 nm, d) WP-1 at 512 nm, e) WP-2 at 406nm and f) WP-2 at 512 nm at room temperature.

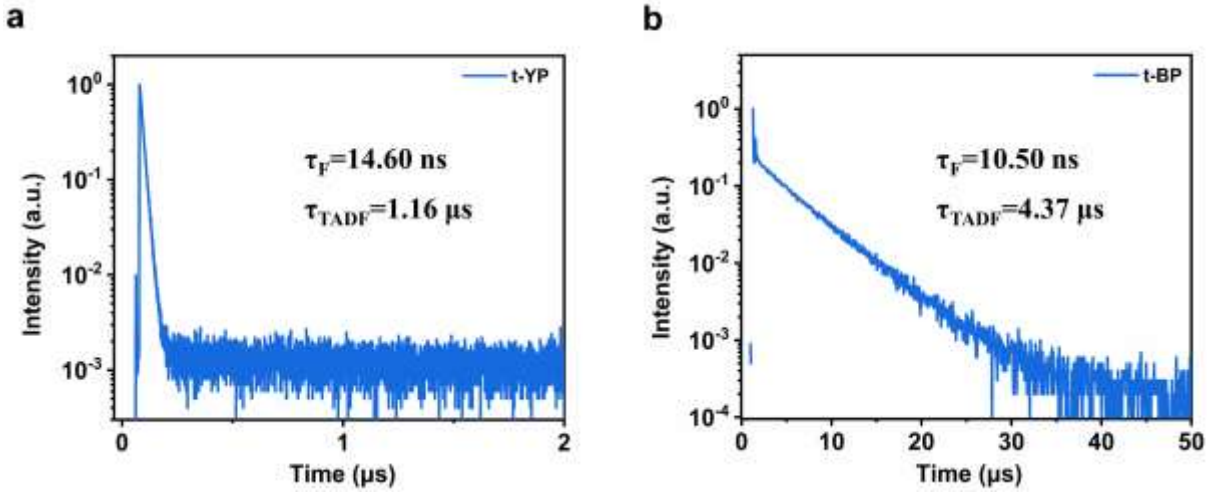

Fig. S13. Transient decay spectra of different samples of **PXZ-DtCzBN**: a) t-YP and b) t-BP at room temperature.

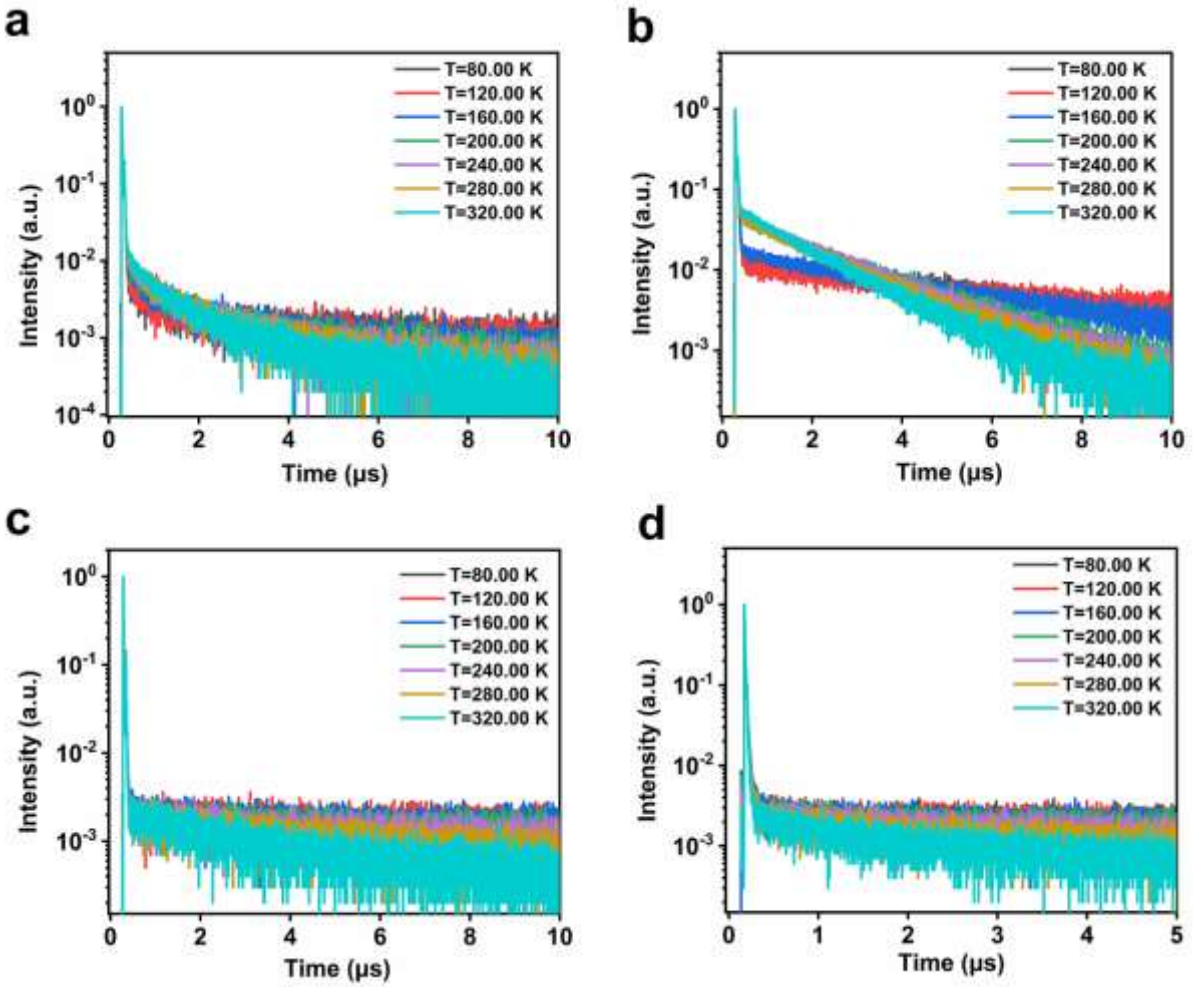

Fig. S14. Transient PL decay curves of different samples of **PXZ-DCzBN** a) YP, b) GP, c) WP-1 at 512 nm and d) WP-2 at 512 nm measured at 80-320K.

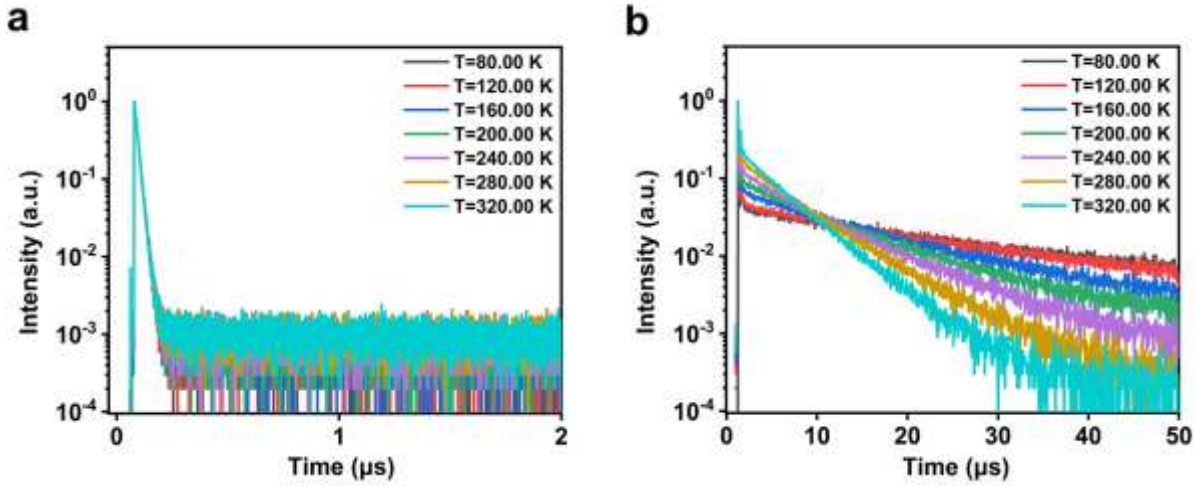

Fig. S15. Transient PL decay curves of different samples of **PXZ-DtCzBN** a) t-YP and b) t-BP measured at 80-320K.

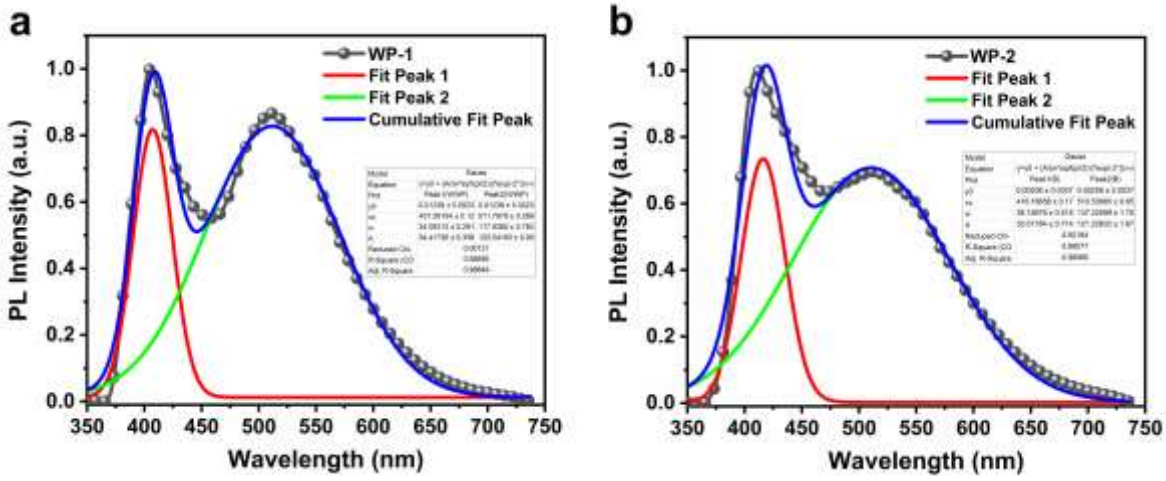

Fig. S16. The multiple peak fit results of the PL spectra of **PXZ-DCzBN**: a) WP-1 and b) WP-2 utilized to calculate the PLQY values of short-wavelength and long-wavelength emission.

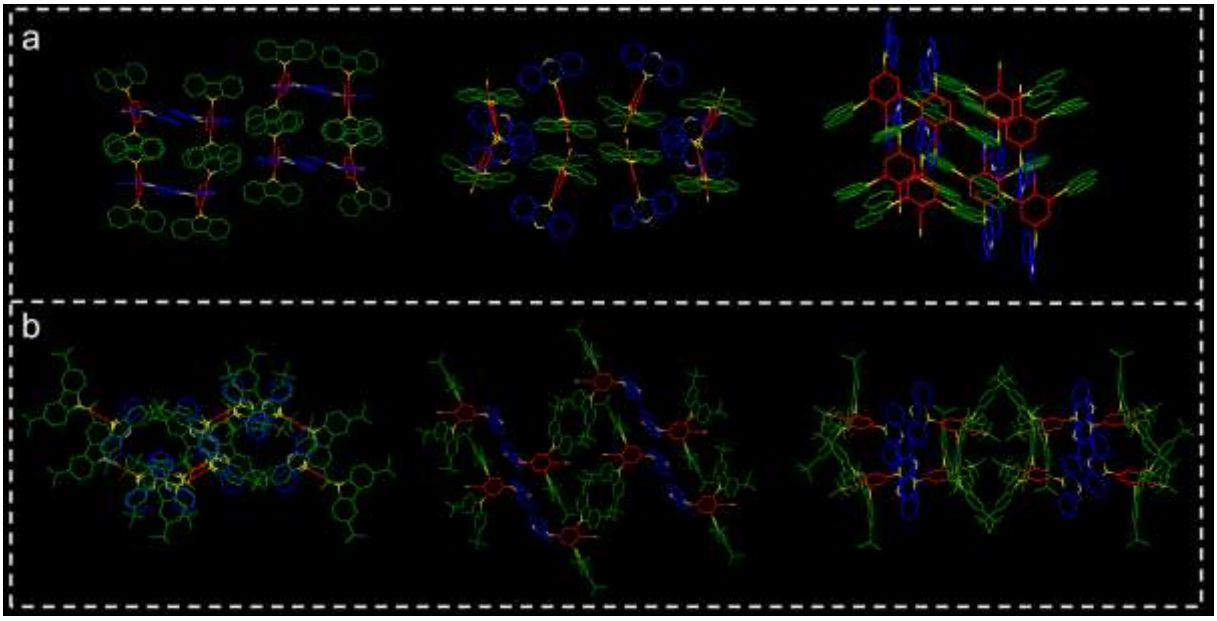

Fig. S17. Molecular packing modes of a) **PXZ-DCzBN** and b) **PXZ-DtCzBN** crystals from different views.

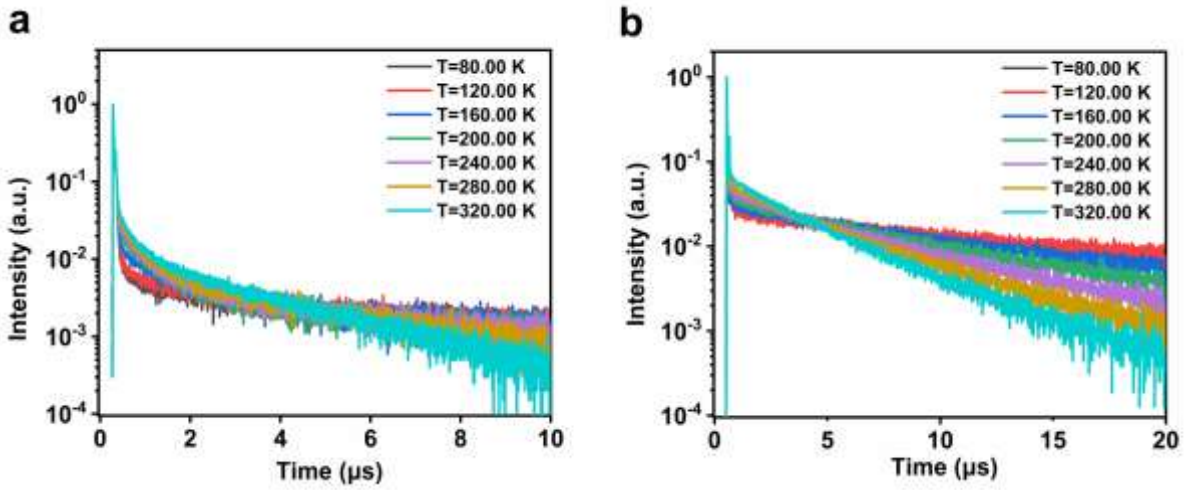

Fig. S18. Transient PL decay curves of a) **PXZ-DCzBN** crystals and b) **PXZ-DtCzBN** crystals measured at 80-320K.

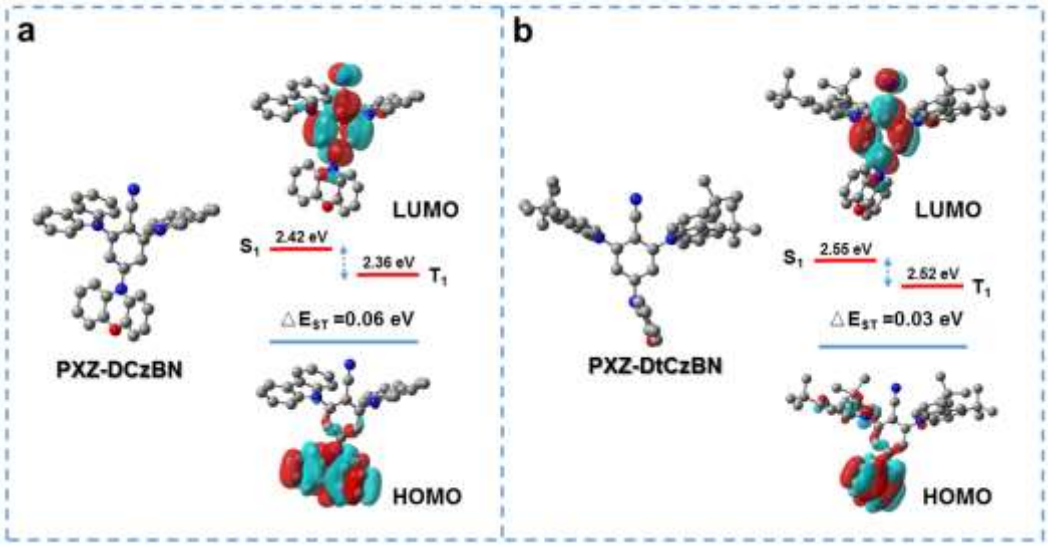

Fig. S19. DFT and TD-DFT calculation results with single crystal structures of a) **PXZ-DCzBN** and b) **PXZ-DtCzBN** as initial conformation without further optimization.

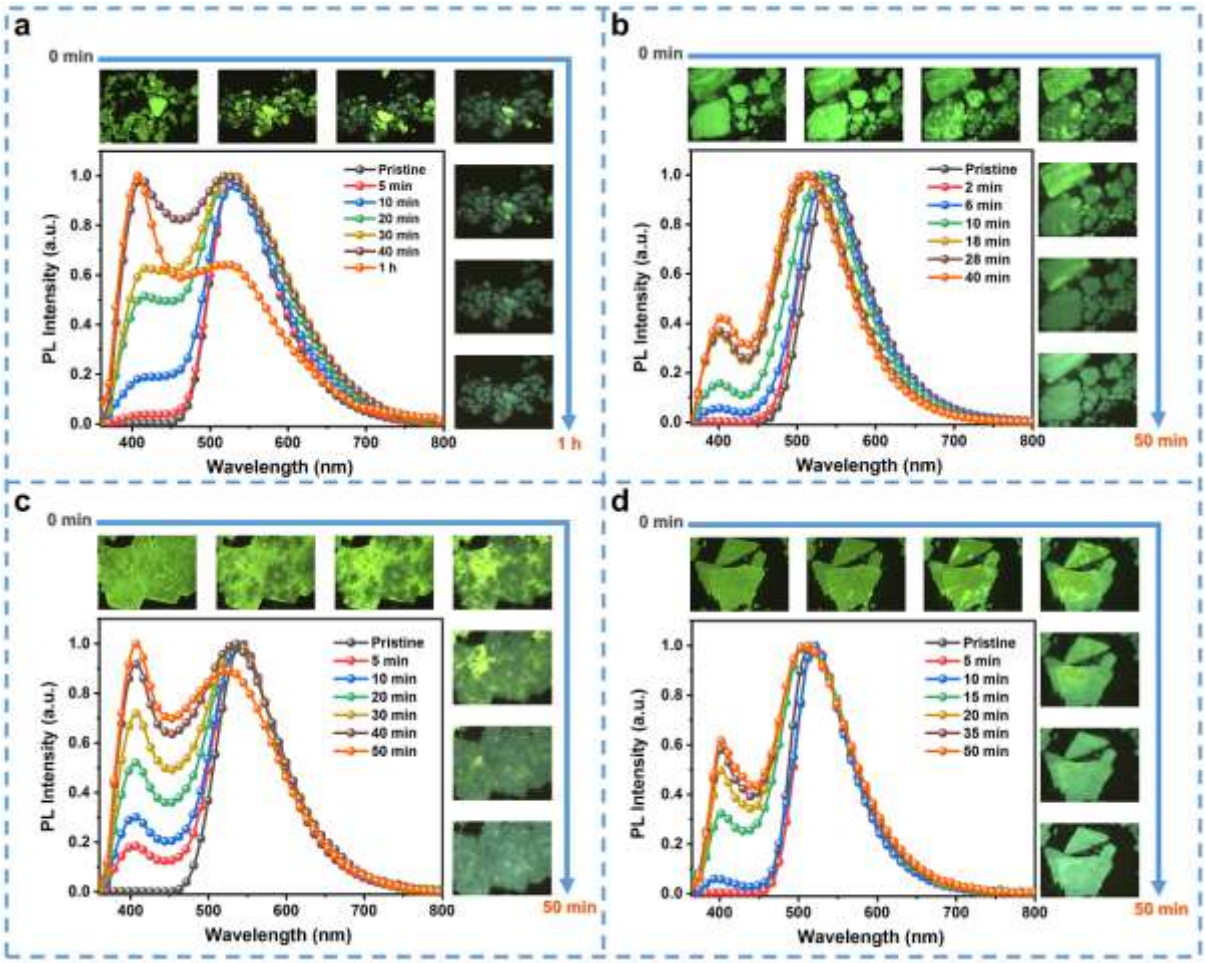

Fig. S20. Results of fluorescence microscopy and CCD spectrometer in situ monitoring of different samples of **PXZ-DCzBN**: GP treated with (a) methanol or (b) hexane, and single crystal treated with (c) methanol or (d) hexane.

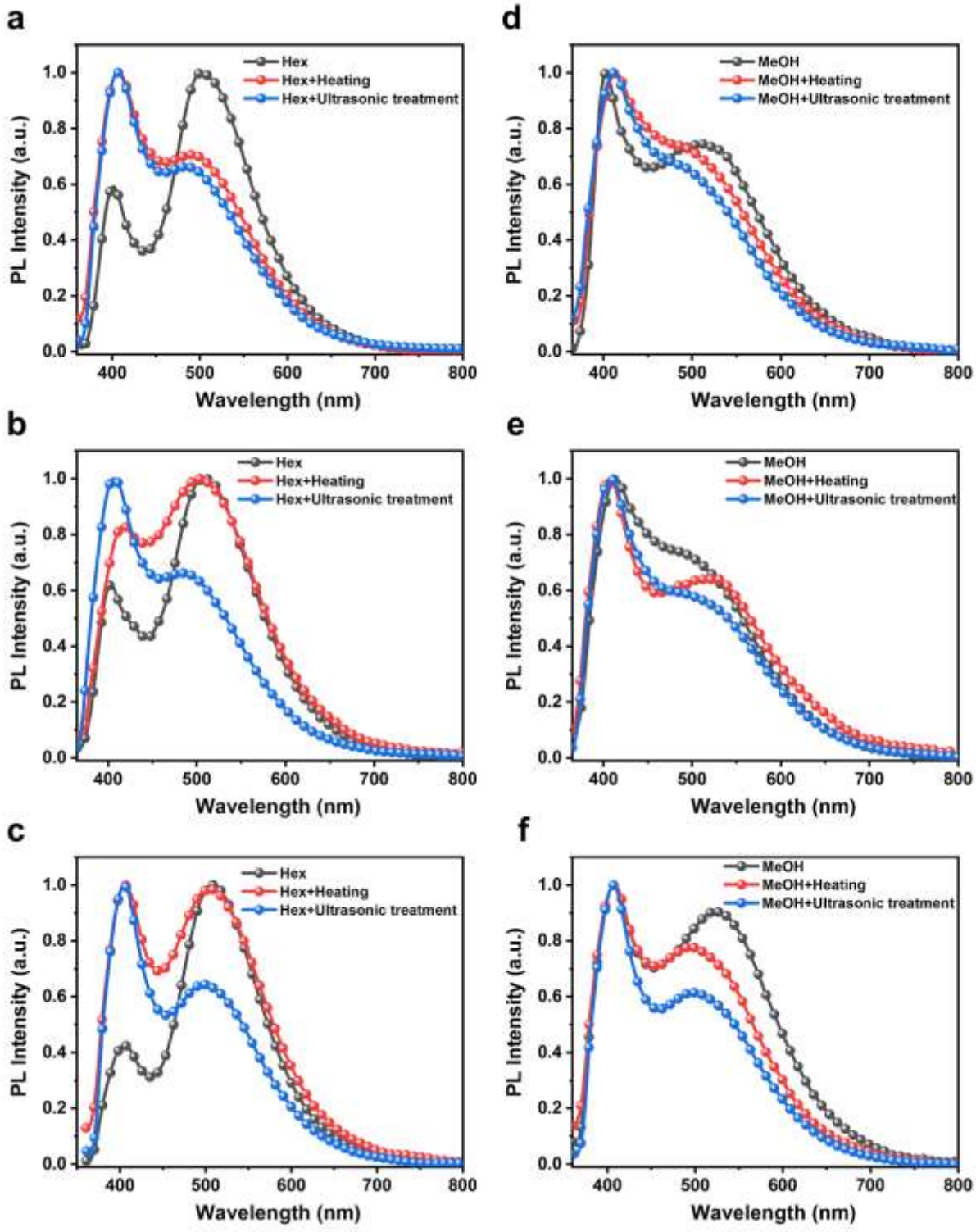

Fig. S21. Under different conditions, the final PL spectra of a)YP, b)GP and c) single crystal of **PXZ-DCzBN** treated with hexane, and final PL spectra of d)YP, e)GP and f) single crystal of **PXZ-DCzBN** treated with methanol.

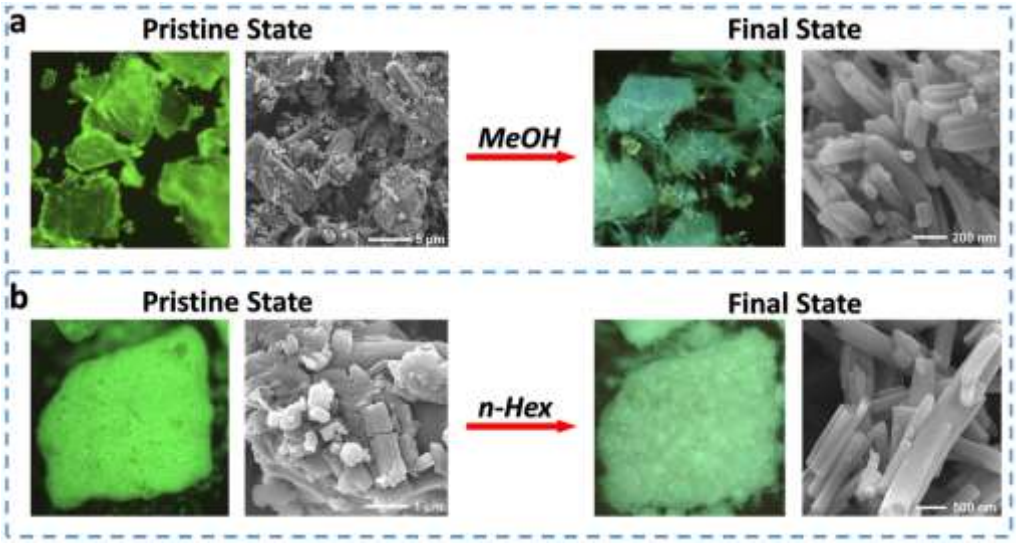

Fig. S22. The magnified fluorescence microscopy and SEM images before and after GP (**PXZ-DCzBN**) was treated with (a) methanol or (b) hexane.

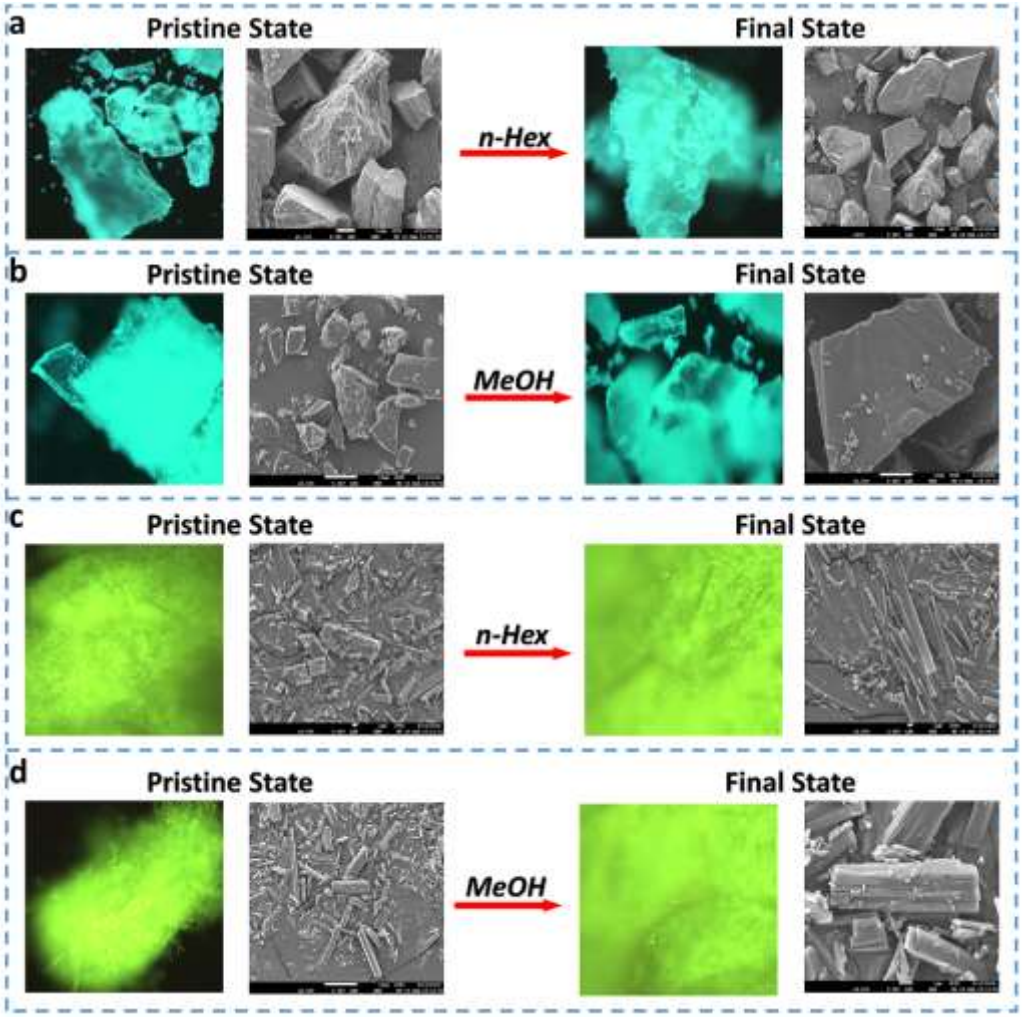

Fig. S23. The magnified fluorescence microscopy and SEM images of different samples of **PXZ-DtCzBN**: before and after t-BP was treated with (a) hexane or (b) methanol, and t-YP was treated with (c) hexane or (d) methanol.

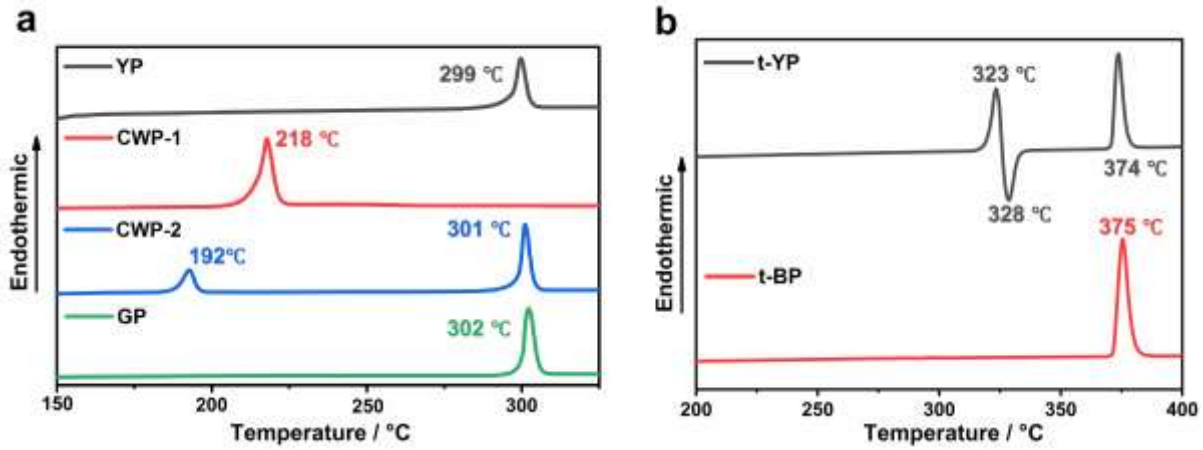

Fig. S24. DSC curves of (c) **PXZ-DCzBN** and (d) **PXZ-DtCzBN**.

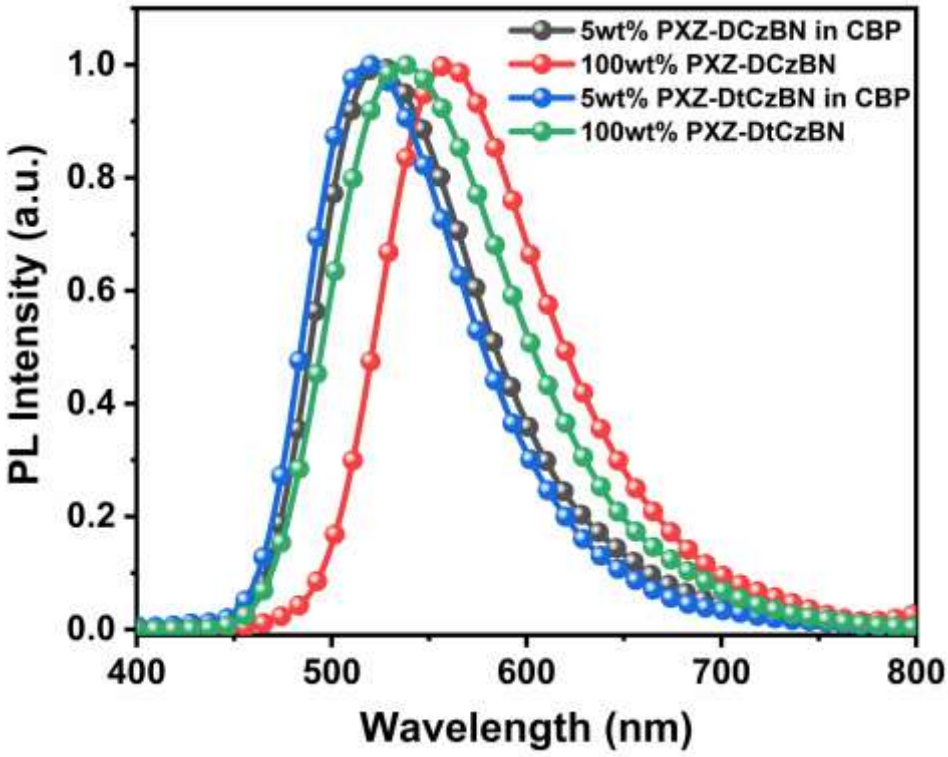

Fig. S25. The fluorescence spectra of doped and non-doped film constructed by **PXZ-DCzBN** and **PXZ-DtCzBN** at 298 K.

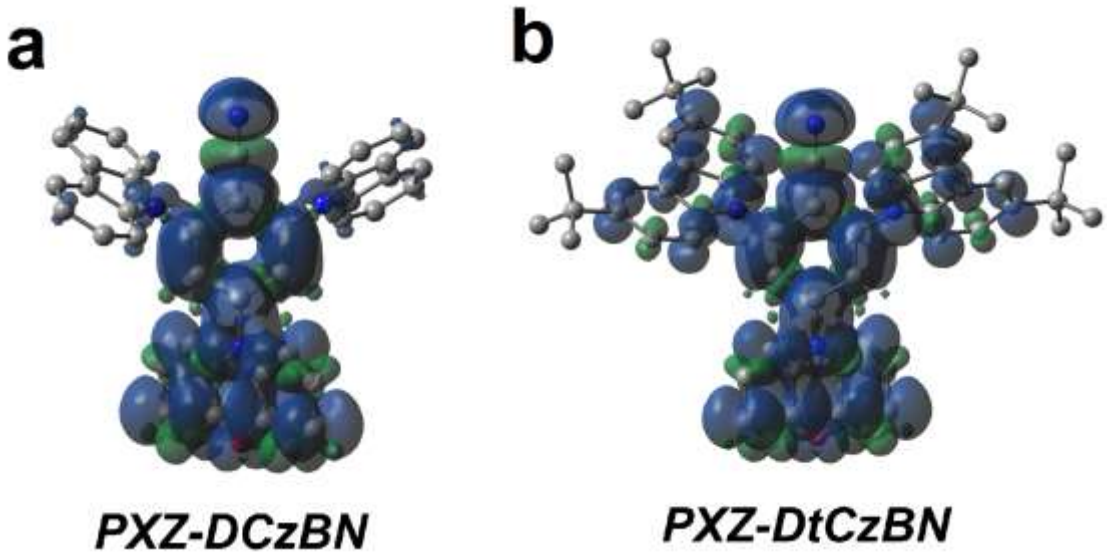

Fig. S26. Spin density distributions of T_1 states of **PXZ-DCzBN** and **PXZ-DtCzBN**.

4. Tables:

Table S1. Detailed photophysical data of **PXZ-DCzBN** and **PXZ-DtCzBN** in solution and films.

Photophysical Parameters	Compound					
	PXZ-DCzBN			PXZ-DtCzBN		
	5% in CBP	Neat film	Toluene solution	5% in CBP	Neat film	Toluene solution
λ_{em}[a] [nm]	524	559	528	519	536	528
Φ_{PL}[b] [%]	56	48	33	66	50	26
Φ_{F}[c] [%]	29.7	29.7	12.7	16.3	26.6	7.4
Φ_{TADF}[d] [%]	26.4	18.3	20.3	49.7	23.4	18.6
τ_{F}[e] [ns]	19.23	18.02	20.65	19.43	21.62	21.96
τ_{TADF}[f] [μs]	1.31	0.82	1.51	2.72	1.07	1.71
k_{F}[g] [10^7 s^{-1}]	1.54	1.65	0.62	0.84	1.23	0.34
k_{ISC}[h] [10^7 s^{-1}]	3.66	3.90	4.23	4.31	3.39	4.22
k_{TADF}[i] [10^5 s^{-1}]	2.86	3.16	1.54	2.19	2.99	1.18
k_{RISC}[j] [10^6 s^{-1}]	0.96	1.06	1.21	1.34	1.12	1.59
Φ_{ISC}[k] [%]	70.4	70.3	87.3	83.7	73.4	92.6
Φ_{RISC}[l] [%]	37.5	26.0	23.2	59.4	31.8	20.1

[a]Emission maxima. [b]The total fluorescence quantum yield. [c]The prompt fluorescent (Φ_F) component of Φ_{PL}. [d]The delayed fluorescent (Φ_{TADF}) component of Φ_{PL}. [e]The lifetimes of prompt fluorescent (τ_P). [f]The lifetimes of TADF (τ_D). [g]The rate constants of fluorescent (k_F). [h]The rate constants of TADF (k_{TADF}). [i]The rate constants of intersystem crossing (k_{ISC}). [j]The rate constants of reverse intersystem crossing (k_{RISC}). [k]The efficiency of ISC(Φ_{ISC}). [l]The efficiency of RISC (Φ_{RISC}).

Table S2. Detailed photophysical data of different **PXZ-DCzBN** and **PXZ-DtCzBN** solid samples.

Photophysical Parameters	Compound					
	PXZ-DCzBN				PXZ-DtCzBN	
	YP	GP	WP-1*	WP-2*	t-YP	t-BP
λ_{em}[a] [nm]	563	518	512	512	543	490
Φ_{PL}[b] [%]	16	29	5	4	30	48
Φ_{F}[c] [%]	10	7	4	2	29	~0
Φ_{TADF}[d] [%]	6	22	1	2	1	48
τ_{F}[e] [ns]	23.98	26.56	10.36	13.76	14.60	10.50
τ_{TADF}[f] [μs]	1.05	1.23	1.23	1.15	1.16	4.37
k_{F}[g] [10^6 s^{-1}]	4.09	2.52	3.63	1.64	19.72	~0
k_{ISC}[h] [10^7 s^{-1}]	3.76	3.51	9.29	7.10	4.88	9.38
k_{TADF}[i] [10^4 s^{-1}]	6.54	19.4	1.04	1.55	1.46	10.8
k_{RISC}[j] [10^5 s^{-1}]	6.66	29.0	2.77	6.89	5.08	70.7
Φ_{ISC}[k] [%]	90.2	93.3	96.2	97.7	71.2	98.5
Φ_{RISC}[l] [%]	6.9	23.9	1.28	1.78	1.70	47.2

[a]Emission maxima. [b]The total fluorescence quantum yield. [c]The prompt fluorescent (Φ_F) component of Φ_{PL}. [d]The delayed fluorescent (Φ_{TADF}) component of Φ_{PL}. [e]The lifetimes of prompt fluorescent (τ_P). [f]The lifetimes of TADF (τ_D). [g]The rate constants of fluorescent (k_F). [h]The rate constants of TADF (k_{TADF}). [i]The rate constants of intersystem crossing (k_{ISC}). [j]The rate constants of reverse intersystem crossing (k_{RISC}). [k]The efficiency of ISC(Φ_{ISC}). [l]The efficiency of RISC (Φ_{RISC}). *Considering only the emission of 512 nm of CWP and WWP featured with TADF characteristic, we only calculated the photophysical data of 512 nm emission here. And the Φ_{PL} here is calculated from the multiple peak fit results.

Table S3. Crystal data of **PXZ-DCzBN**.

Empirical formula	$C_{43}H_{26}N_4O$
Formula weight	614.68
Temperature/K	150(2)
Crystal system	triclinic
Space group	P-1
a/Å	13.2950(7)
b/Å	16.9126(10)
c/Å	33.4253(19)
α/°	94.049(2)
β/°	96.201(2)
γ/°	90.124(2)
Volume/Å^3	7452.8(7)
Z	8
ρcalcg/cm^3	1.096
μ/mm-1	0.067
F(000)	2560
Crystal size/mm^3	0.200 × 0.200 × 0.050
Radiation	MoKα (λ = 0.71073)
2Θ range for data collection/°	5.476 to 50
Index ranges	-15 ≤ h ≤ 15, -19 ≤ k ≤ 20, -39 ≤ l ≤ 39
Reflections collected	77635
Independent reflections	26225 [Rint = 0.0529, Rsigma = 0.0750]
Data/restraints/parameters	26225/3072/1729
Goodness-of-fit on F2	1.065
Final R indexes [I>=2σ (I)]	R1 = 0.0596, wR2 = 0.1446
Final R indexes [all data]	R1 = 0.0987, wR2 = 0.1577
Largest diff. peak/hole / e Å^{-3}	0.21/-0.24

Table S4. Crystal data of **PXZ-DtCzBN**.

Empirical formula	$C_{59}H_{58}N_4O$
Formula weight	839.09
Temperature/K	100(2)
Crystal system	monoclinic
Space group	C2/c
a/Å	38.7107(19)
b/Å	11.7637(6)
c/Å	21.4913(10)
α/°	90
β/°	98.148(3)
γ/°	90
Volume/Å^3	9687.9(8)
Z	8
ρcalcg/cm^3	1.151
μ/mm^{-1}	0.068
F(000)	3584
Crystal size/mm^3	0.140 × 0.130 × 0.120
Radiation	MoKα (λ = 0.71073)
2Θ range for data collection/°	5.776 to 51.998
Index ranges	$-47 \leq h \leq 47$, $-14 \leq k \leq 14$, $-26 \leq l \leq 26$
Reflections collected	63220
Independent reflections	9515 [Rint = 0.0714, Rsigma = 0.0460]
Data/restraints/parameters	9515/1008/589
Goodness-of-fit on F2	1.015
Final R indexes [I>=2σ (I)]	R1 = 0.0509, wR2 = 0.1037
Final R indexes [all data]	R1 = 0.0758, wR2 = 0.1142
Largest diff. peak/hole / e Å^{-3}	0.24/-0.29

5. References

[1] Becke, A. D. Density-functional thermochemistry. III. The role of exact exchange. The Journal of Chemical Physics 1993, 98 (7), 5648-5652.

[2] Lee, C.; Yang, W.; Parr, R. G. Development of the Colle-Salvetti correlation-energy formula into a functional of the electron density. Physical Review B 1988, 37 (2), 785-789.

[3] Krishnan, R.; Binkley, J. S.; Seeger, R.; Pople, J. A. Self-consistent molecular orbital methods. XX. A basis set for correlated wave functions. The Journal of Chemical Physics 1980, 72 (1), 650-654.

[4] Grimme, S.; Antony, J.; Ehrlich, S.; Krieg, H. A consistent and accurate ab initio parametrization of density functional dispersion correction (DFT-D) for the 94 elements H-Pu. J Chem Phys 2010, 132 (15), 154104.

[5] Frisch, M. J.; Trucks, G. W.; Schlegel, H. B.; Scuseria, G. E.; Robb, M. A.; Cheeseman, J. R.; Scalmani, G.; Barone, V.; Petersson, G. A.; Nakatsuji, H.; Li, X.; Caricato, M.; Marenich, A. V.; Bloino, J.; Janesko, B. G.; Gomperts, R.; Mennucci, B.; Hratchian, H. P.; Ortiz, J. V.; Izmaylov, A. F.; Sonnenberg, J. L.; Williams-Young, D.; Ding, F.; Lipparini, F.; Egidi, F.; Goings, J.; Peng, B.; Petrone, A.; Henderson, T.; Ranasinghe, D.; Zakrzewski, V. G.; Gao, J.; Rega, N.; Zheng, G.; Liang, W.; Hada, M.; Ehara, M.; Toyota, K.; Fukuda, R.; Hasegawa, J.; Ishida, M.; Nakajima, T.; Honda, Y.; Kitao, O.; Nakai, H.; Vreven, T.; Throssell, K.; Montgomery, J. A., Jr.; Peralta, J. E.; Ogliaro, F.; Bearpark, M. J.; Heyd, J. J.; Brothers, E. N.; Kudin, K. N.; Staroverov, V. N.; Keith, T. A.; Kobayashi, R.; Normand, J.; Raghavachari, K.; Rendell, A. P.; Burant, J. C.; Iyengar, S. S.; Tomasi, J.; Cossi, M.; Millam, J. M.; Klene, M.; Adamo, C.; Cammi, R.; Ochterski, J. W.; Martin, R. L.; Morokuma, K.; Farkas, O.; Foresman, J. B.; Fox, D. J. Gaussian 09, Revision D.01, Gaussian, Inc., Wallingford, CT 2013.

[6] G.M. Sheldrick, *Acta Crystallogr A Found Adv*, **2015**, 71, 3-8

[7] G.M. Sheldrick, *Acta Crystallogr C Struct Chem*, **2015**, 71, 3-8

[8] Q. Zhang, H. Kuwabara, W. J. Potscavage, S. Huang, Y. Hatae, T. Shibata, C. Adachi, *J. Am. Chem. Soc*. **2014**, 136, 18070-18081.